Available online at www.sciencedirect.com

ScienceDirect

Procedia CIRP 117 (2023) 225–230

www.elsevier.com/locate/procedia

19th CIRP Conference on Modeling of Machining Operations

Simulation-based analysis of electrical current induction in electrochemical precision machining of Nd-Fe-B permanent magnets

Alexander Thielecke[a,*], Matthias Hackert-Oschätzchen[a], Nasibullo Komilov[a], Gunnar Meichsner[a], Tom Petzold[b], Sascha Loebel[b], André Martin[b], Robin Schulze[c], Andreas Schubert[b]

[a] *Chair of Manufacturing Technology with Focus Machining, Institute of Manufacturing Technology and Quality Management (IFQ), Faculty of Mechanical Engineering, Otto von Guericke University Magdeburg, 39106 Magdeburg, Germany*

[b] *Professorship Micromanufacturing Technology, Chemnitz University of Technology, 09107 Chemnitz, Germany*

[c] *SITEC Industrietechnologie GmbH, 09114 Chemnitz*

* Corresponding author. Tel.: +49-391-67-57596 ; fax: +49-391-67-42370. *E-mail address:* alexander.thielecke@ovgu.de

Abstract

Permanent magnets are machined by Electrical Discharge Machining. The thermal influence on the workpieces can affect the magnetic properties. Therefore, the magnetisation of the material is performed in a subsequent processing step.
Pulsed Electrochemical Machining (PECM) represents a potential alternative. It is expected that the oscillation of the cathode leads to electrical current induction, which affects the electric current density on the workpiece surface.
In this study, the electrical current induction when machining Nd-Fe-B with PECM is analysed based on simulation. Based on the results, recommendations of process input variables for the PECM process can be derived.

Keywords: Pulsed electrochemical machining (PECM); Multiphysics simulation; Electromagnetic induction; Permanent magnets

1. Introduction

ECM was identified as an alternative to avoid the negative influence on the magnetic properties of permanent magnets, and thus represents an alternative machining technique with negligible thermal influences other than established EDM processes. As a consequence, subsequent magnetisation is no longer necessary, which would significantly increase production efficiency. ECM uses the principle of electrolysis, in which an anodically polarized workpiece is machined by applying an electric current. The gap between the two electrodes should be kept small in a defined manner in order to transfer the shape of the tool into the workpiece with high precision and to minimize the ohmic voltage drop between the cathode and anode for high economic efficiency. As charge carrier, an electrolyte solution is pumped through the working gap, which continuously removes the generated heat as well as gaseous, dissoluted and solid removal products. [1] In order to make the ECM process more precise, the PECM process was developed, in which the accuracy of the process and the surface quality of the workpieces could be further increased with pulsed direct current and an oscillating cathode [2, 3]. The examined alloy Nd-Fe-B has excellent magnetic properties, such as high magnetic energy product, coercivity and energy density. Among the commercially available permanent magnets, it is the material with the strongest magnetisation $(BH)_{max}$ [4]. Areas of application include advanced engine and drive systems [5]. The influence of the magnetic field on the test specimens examined according to DIN SPEC 91399 [6, 7] was analysed using the simulation software COMSOL Multiphysics Version 6.0. The presentation of the results focuses on the current density distribution in the PECM device, which strongly influences the removal of the material and thus the efficiency of the PECM Process.

* Corresponding author

2. Electromagnetic induction

The coupling between the electric and magnetic fields is explained by Faraday's Law of Electromagnetic Induction given

2212-8271
10.1016/j.procir.2023.03.039

in Equation 1, which shows the relation between the electric and magnetic fields [8].

$$\nabla \times \mathbf{E} = -\frac{\partial \mathbf{B}}{\partial t} \tag{1}$$

Equation 1 also indicates that Faraday's law is general and independent of the geometry. As can be seen in Fig. 1, a time-varying magnetic flux density can induce a current in any conductive volume such as a cathode.

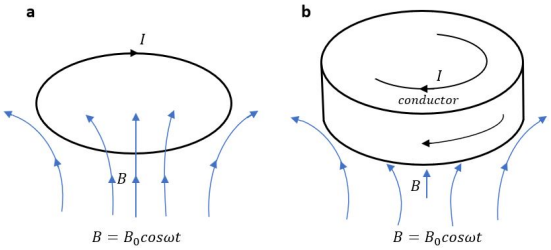

Fig. 1: (a) A time-dependent flux density generates an induced current in a loop; (b) The same in a conducting volume [8]

Based on Faraday's Law of Electromagnetic Induction, it is assumed that the oscillating movement of the cathode back and forth relative to the permanent magnetic workpiece has an influence on the current density distribution in the PECM process.

3. Model description

3.1. Geometry and materials

The design concept for the PECM model was adapted from previous ablation experiments of the magnetic material Nd-Fe-B [6, 9]. Fig. 2 shows the designed model with domain definitions in the simulation software. Due to the almost rotationally symmetrical device, the model was designed as two-dimensional geometry with the axis of symmetry at X = 0. The two electrodes can be seen in yellow (cathode) and gray (anode), the respective contacts in shades of yellow and purple, and the lower and upper part of the flushing chamber made of insulating material in green. The colouring, arrangement and geometric dimensions of cathode and workpiece correspond to DIN SPEC 91399. Both electrodes are cylindrical in shape. The workpiece has a diameter of 12 mm and a length of 45 mm. The cathode consists of a stepped shaft with diameters of 7.5 mm and 12 mm and a length of 37.5 mm. The oscillating movement of the tool unit occures in Z-direction.

The anode (I) consists of the magnetic material Nd-Fe-B. For the cathode (II), stainless steel 1.4301 was selected, because it is a non-ferromagnetic austenitic steel, meaning that the magnetic force on the cathode movement will be negligible. As a non-solid material, domain III represents the electrolyte. Table 1 summarises the materials for each domain and their material parameters. For the analysis of the induction, the electrical conductivity σ, the relative permeability μ_r and the relative permittivity ϵ_r are assigned to the domains.

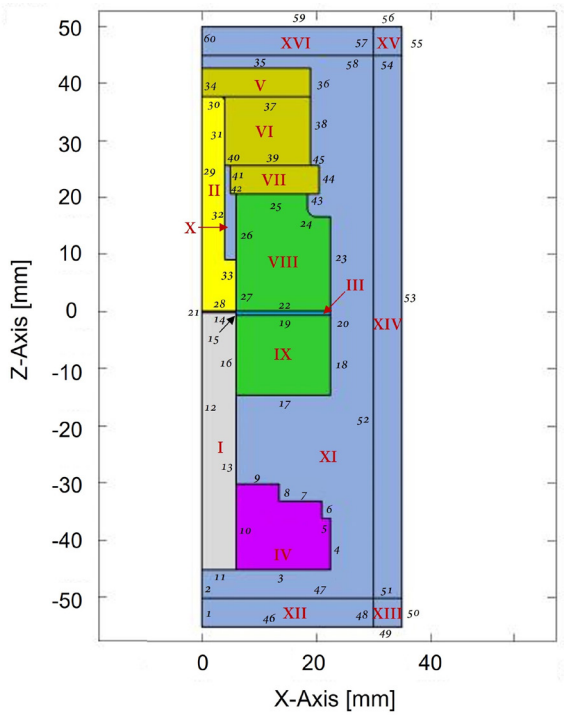

Fig. 2: 2D axisymmetric model geometry with defined domains

Table 1: Material parameters of the simulation model

Domain	Material	σ [S/m]	μ_r	ϵ_r
I	NdFeB	$6.67 \cdot 10^5$	1.05	1.05
II, IV-VII	1.4301	$7.3 \cdot 10^5$	1.02	1
III	Electrolyte ($NaNO_3$)	7	0.28	1
VIII, IX	PMMO	10^{-10}	1	4
X-XVI	Air	$3 \cdot 10^{-15}$	1	1.006

3.2. Physics and boundary conditions

3.2.1. Magnetic field

The physics module Magnetic Fields was applied to magnetise the workpiece domain for further simulations. The target value for calibrating the workpiece is a magnetic flux density of $B = 460 \pm 5$ % on the face of the workpiece. This value was measured in previous experiments on the face of the workpiece geometry with a magnetic field tester PCE-MFM 3000 from PCE Deutschland GmbH [9]. The measuring device is equipped with an external Hall sensor and measures static and changing magnetic fields with an accuracy of ± 5 % of the measured value. This value directly affects the magnitude of the induced current. The domain and boundary conditions of the magnetic field module are listed and described in Table 2.

3.2.2. Moving mesh

Moving mesh mode is implemented to simulate the oscillation of the cathode, including relevant domains such as the cathode contact, the upper and the lower insulation. The oscillation can

Table 2: Domain and boundary conditions of magnetic field

Domain Condition	Domain	Property
Ampere's Law 1	all	μ_r from material (Tab. 1)
Initial Values	all	Magnetic vector potential $A_x = 0$; $A_\varphi = 0$; $A_z = 0$ [Wb/m]
Ampere's Law 2	I	Magnetisation model: Remanent flux density $B_r = 1$ [T] Remanent flux direction $e_x = 0$; $e_\varphi = 0$; $e_z = 1$ [T]

Boundary Condition	Boundary	Property
Axial Symmetry	1, 2, 12, 21, 29, 34, 60, 61	-
Magnetic Isolation	46, 49, 50, 53 55, 56, 59	-

be described with a time-dependent sinus function as provided in Equation 2.

$$z(t) = -\widehat{z} \cdot \sin(2\pi \cdot f_z \cdot t) \tag{2}$$

Due to the negative sign, the starting movement of the cathode is directed downwards towards the workpiece. Since $f(t)$ is a wave function, it oscillates with a frequency f of 50 Hz and an amplitude $\widehat{z}$ of 185 µm between the lowest and highest peaks, and the peak-to-peak amplitude $\triangle Z$ is equal to 370 µm. Table 3

Table 3: Oscillation parameters of the cathode

Description	Symbol	Value	Unit
Frequency	f	50	[Hz]
Period	T	20	[ms]
Amplitude	$\widehat{z}$	185	[µm]
Peak-to-peak Amplitude	$\triangle Z$	370	[µm]
Working distance	a	70	[µm]

lists the oscillation parameters used for the movement of the cathode. Fig. 3 illustrates the oscillation movement of the cathode with a sinus wave function $z(t)$ passing through the phases I-V over a time of 20 ms. Domain and boundary conditions of moving mesh module are listed and described in Table 4.

3.2.3. Electric current

Electric current mode was applied to supply the PECM process with external electric potential. An important characteristic of this simulation model is that a pulsed electric potential $U_{\text{pulsed}}(t)$ needs to be defined. To connect a time-dependent switching current, a rectangle function was implemented. This function applies the electrical potential U in the interval of a lower t_{Low}

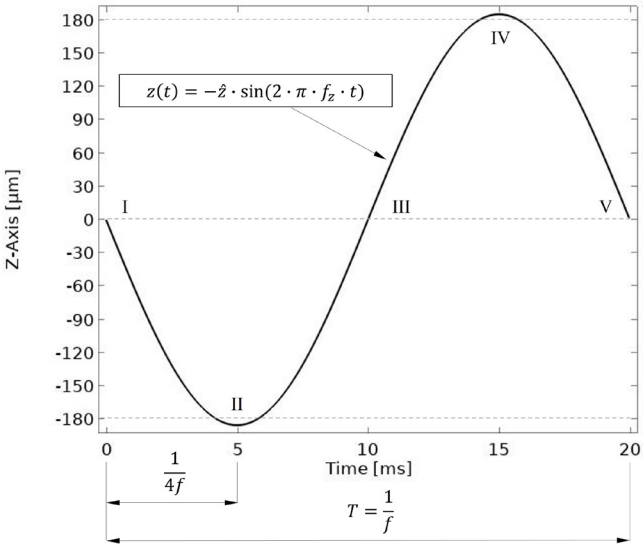

Fig. 3: Principle representation of cathode oscillation over time

Table 4: Domain and boundary conditions of moving mesh

Domain Condition	Domain	Property
Prescribed Deformation	I, IV, XII-XVI	$d_x = 0$; $d_z = 0$
Deforming Domain	II, III, V - XI	Initial deformation $d_x = 0$; $d_z = 0$

Boundary Condition	Boundary	Property
Fixed Boundary	3, 5, 7, 9, 14, 47, 58	-
Prescribed Mesh Displacement in Normal Direction	2, 4, 6, 8, 13 15, 20, 21, 52, 61	$d_n = 0$
Prescribed Mesh Displacement	16 - 19, 22 - 45	$d_x = 0$; $d_z = -\widehat{z} \cdot \sin(2\pi \cdot f_z \cdot t)$

and an upper t_{Upp} limit of the rectangle function as shown in the Equation 3 and Equation 4.

$$t_{Low} = \frac{T}{4} - \frac{t_p}{2} \tag{3}$$

$$t_{Upp} = \frac{T}{4} + \frac{t_p}{2} \tag{4}$$

The Equation 5 explains the pulsed electric potential $U_{\text{pulsed}}(t)$ which connects and disconnects the voltage according to the lower and upper time limits.

$$U_{pulsed}(t) = \begin{cases} 0\ \text{V}, & \text{if} \quad t < t_{Low} \\ 10\ \text{V}, & \text{if} \quad t_{Low} \leq t \leq t_{Upp} \\ 0\ \text{V}, & \text{if} \quad t > t_{Upp} \end{cases} \tag{5}$$

The pulsed current parameters used in the simulation model are summarized in the Table 5 below.

Table 5: Pulsed electric potential parameters [9]

Description	Symbol	Value	Unit
Pulse width	t_p	4	[ms]
Lower limit	t_{Low}	3	[ms]
Upper limit	t_{Upp}	7	[ms]
Baseline	U_0	0	[V]
Electric Potential Amplitude	U	10	[V]

Fig. 4 illustrates the cathode oscillation and a pulsed electrical potential in two periods, here the oscillation graph $f(t)$ marked with dark line is plotted as in Eq. 2 (also shown in Fig. 3) and the pulsed voltage $U_{pulsed}(t)$ graph marked with red line is characterized as in Eq. 5. This function is achieved via the switching electric potential $U_{pulsed}(t)$ ranging from 0 V to 10 V with the pulse width t_p of 4 ms.

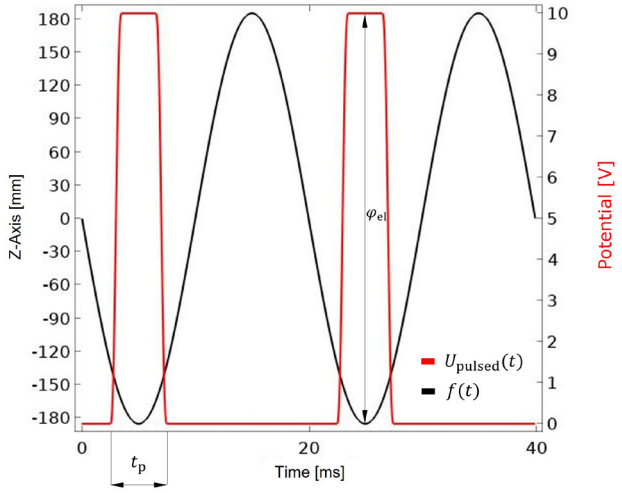

Fig. 4: Cathode oscillation and pulsed potential in two periods

The domains I-VII in electric current mode are selected for current conservation and electric conductivity σ of the materials are used from the Table 1. While the anode contact boundary 3 has been assigned to the electric potential $\varphi_{el} = U_{pulsed}(t)$, the cathode contact boundary 35 has been defined as ground. Domain and boundary conditions of electric current mode defined in the PECM simulation model are listed in the Table 6.
A potential source of error is the influence of meshing accuracy. A mesh sensitivity analysis was performed. For this purpose, several meshes of different fineness were analyzed to exclude calculation errors. The mesh for the model to study the influence of the magnetic field on the PECM process was generated using a physics-controlled mesh as a sequence type. The maximum element size is 5.5 mm, the minimum element size is 0.03 mm. The meshed geometry has a total number of 4628 elements and 2504 mesh vertices. Domains I-XI were meshed with 4383 triangular elements and the infinite air Domains XII-XVI with 245 quadrilateral elements.

Table 6: Domain and boundary conditions of electric current

Domain Condition	Domain	Property
Current Conservation	I - VII	σ from material Tab. 1
Initial Values	I - VII	$\varphi_{el} = 0$ [V]
Boundary Condition	**Boundary**	**Property**
Axial Symmetry	12, 21, 29, 34	-
Electric Insulation	4 - 9, 11, 13, 16, 19, 20, 22, 27, 32, 33, 35 - 38, 40 - 45	-
Ground	35	$\varphi_{el} = 0$ [V]
Electrical Potential	3	$\varphi_{el} = U_{pulsed}(t)$ from Eq. 5 $U_0 = 0$; $U = 10$ [V]

4. Results of the Simulation

In Fig. 5, the magnetic flux density of the model with magnetic field lines at time t = 5 ms is shown. It can be seen that the magnetic flux density is distributed in the geometry and a maximum magnetic flux density B measured in the model amounts to 967 mT.

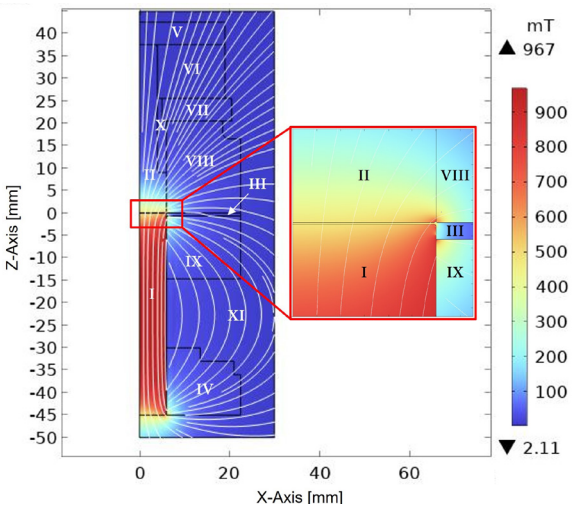

Fig. 5: Magnetic flux density on the anode surface

The magnetic flux density measured on the real specimen, which was studied in previous experiments [6, 9], has been set in the simulation on the surface of the workpiece up to a diameter of around 5 mm, as shown in Fig. 6. The magnetic flux density of the workpiece increases to a diameter of approximately 11 mm to 550 mT and to a maximum value of 765 mT at the outer edge.
Fig. 7 shows the induced current density distribution in the domains of anode, cathode, electrolyte and in the insulation areas.

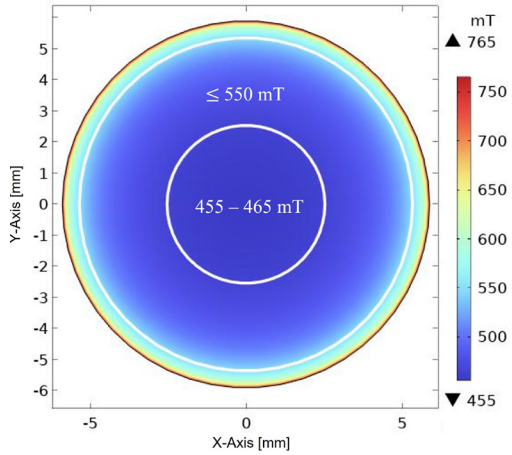

Fig. 6: Magnetic flux density on the anode surface

The current density distribution shown in color scale is solely due to the interaction of the magnetic field from the workpiece and the movement of the cathode without external voltage applied.

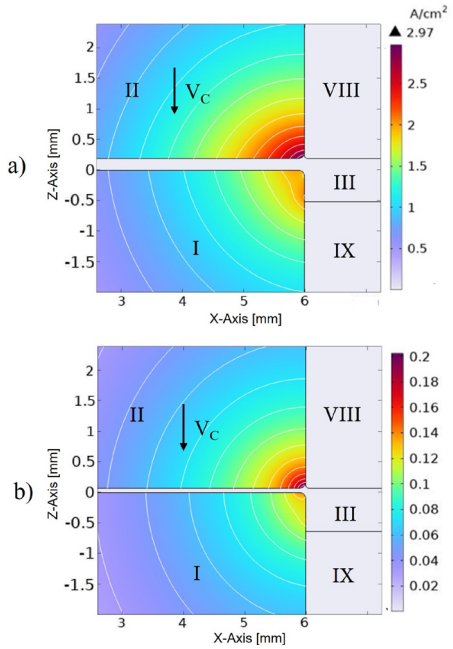

Fig. 7: Induced current density at t = 1 ms (a) and at t = 4.75 ms (b)

As stated in Faraday's law of induction, Fig. 8 shows that the movement of the electrical conductor (cathode) relative to the stationary magnetic field of the workpiece causes an induction current in the domains shown. It can be seen that a current is continuously induced in the electrodes except at the bottom and top dead center of the cathode oscillation.

A maximum current density of 2.97 A/cm^2 is induced at the edge of the cathode surface and a maximum current density of 2.20 A/cm^2 at the edge of the anode surface. A negligible induced current flows in the entire electrolyte area, due to the low electrical conductivity of the electrolyte. Fig. 9 shows the

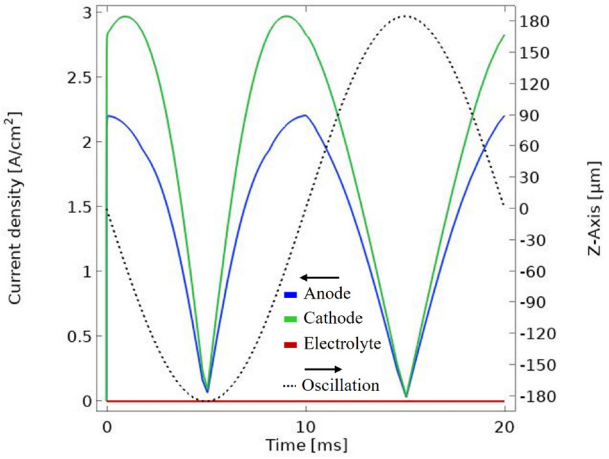

Fig. 8: Maximum induced current density in the volumes of the anode, cathode and electrolyte

current density distribution with switched-on voltage as a comparison to the induced current. The course of the current density

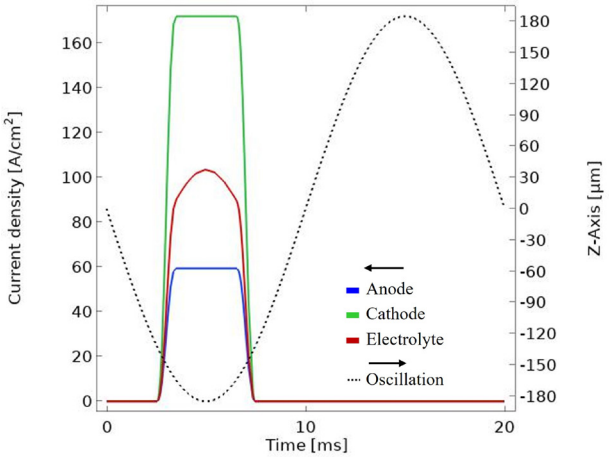

Fig. 9: Maximum electric current density with externally applied voltage in the volumes of the anode, cathode and electrolyte

over time shows that the current density distribution in the overall model assumes a course similar to that of the pulsed electric potential function defined in Eq. 5. The maxima are located on the cathode (between boundaries 42 and 40), electrolyte (27 and 22) and on the anode (13 and 9) at edges that are not significant for the removal process. In addition to the pure amounts of the electrical current density, the direction of the current is decisive for the charge transport, without which there is no removal of the workpiece in the ECM process. For this, the charges have to migrate in the Z-direction of the model. Fig. 10 shows the direction of current in the cathode, electrolyte and anode regions. The induction current flows in a circle (φ-component of cylindrical coordinate system) in the volumes of the anode, cathode and electrolyte. This current is also called eddy current, which is induced in an extended electrical conductor in a time-varying magnetic field or in a moving conductor in a time-constant magnetic field [8]. During U_{pulsed} (t) (Eq.5), the direc-

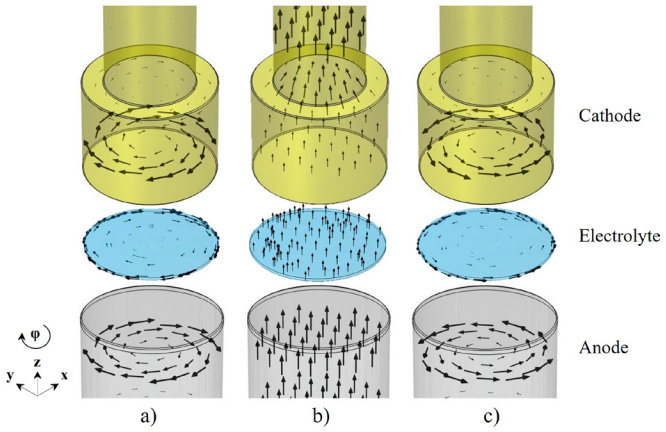

Fig. 10: Current direction at t = 2.5 ms (a), at t = 5 ms (b) and t = 7.5 ms (c)

tion of the current changes with an externally applied voltage in the Z-direction. When the cathode moves upwards from time t = 5 ms and no external voltage is connected, the induction current is again circular but in the opposite direction. Fig. 11 shows that the polarity of the induction current changes depending on the position of the cathode.

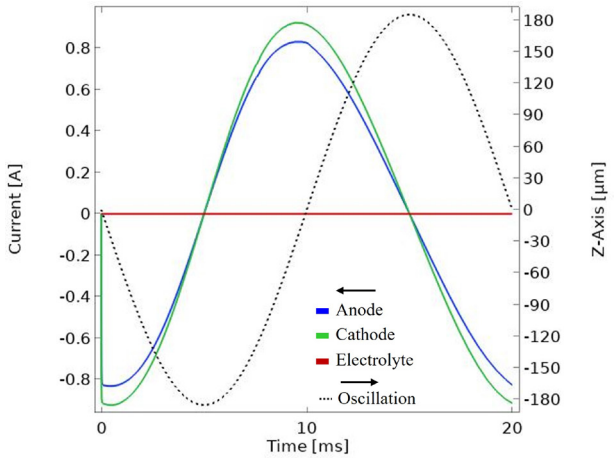

Fig. 11: Induction current in the φ-direction at the surface boundaries of the anode, cathode and in the electrolyte area

In order to ensure the charge transport, that is required for material removal during the ECM process, a temporally constant direct current in the Z-direction must take place. The induction current generated by the changing magnetic field, due to the oscillating cathode, is detected in all domains of the model in the circular (phi) direction. It can be derived, that the induced current, due to the direction of the current flow, does not lead to the removal of the workpiece.

5. Summary and Outlook

In this study, a multiphysical model for simulating the pulsed electrochemical machining of permanent magnets was developed using COMSOL Multiphysics. According to the simulation results, an electrical current induction was detected in the model geometry due to the oscillation movement of the cathode which corresponds with the Faraday's law of induction. The amount of current density induced in this way is significantly lower than the current density generated by the external electric potential. It is expected that the circular direction of the current and in this context the charge transport during the induction current does not lead to a removal of the workpiece. Based on the results of this model, it can be concluded that no adjustments to process input parameters are necessary for PECM experiments with the same test setup and equally strongly magnetised workpiece due to the low and circular flowing induced current. Further experiments and simulations are required to investigate the effects of the induced currents on the state of the electrodes during and after the PECM process. Since the developed model meets the requirements of DIN SPEC 91399 with regard to the geometric dimensions of cathode and workpiece as well as the test arrangement, it can and will be used in the future to investigate material removal on magnetised or non-magnetised workpieces with different input parameters.

Acknowledgements

This project is funded by the Federal Ministry for Economic Affairs and Climate Action, following a decision of the German Bundestag.

References

[1] T. L. Lievestro, "Electrochemical machining," in *ASM handbook*, pp. 533–541, Metals Park, Ohio: ASM International, 1989.
[2] I. Schaarschmidt, M. Hackert-Oschätzchen, G. Meichsner, M. Zinecker, and A. Schubert, "Implementation of the machine tool-specific current and voltage control characteristics in multiphysics simulation of electrochemical precision machining," *Procedia CIRP*, vol. 82, pp. 237–242, 2019.
[3] M. Hackert-Oschätzchen, M. Kowalick, R. Paul, M. Zinecker, D. Kuhn, G. Meichsner, A. Schubert, "2-d axisymmetric simulation of the electrochemical machining of internal precision geometries," *2016 COMSOL Conference in Munich*, 2016.
[4] L. Li, G. Yang, L. Wang, and Q. Wu, "Experimental and theoretical model study on the dynamic mechanical behavior of sintered ndfeb," *Journal of Alloys and Compounds*, vol. 890, p. 161787, 2022.
[5] N.N., "Rare earth permanent magnets," *U.S. Department of Energy Response to Executive Order 14017, "America's Supply Chains"*, 2022.
[6] T. Petzold, A. Martin, A. Schubert, "Electrochemical material removal characteristics of a ndfeb permanent magnet," *euspen's 22nd International Conference & Exhibition, Geneva, CH, May/June 2022*, 2022.
[7] Deutsche Institut für Normung e. V., "Methode zur Bestimmung von Prozesseingangsgrößen für das elektrochemische Präzisionsabtragen - Anforderungen, Kriterien, Festlegungen," 2018.
[8] N. Ida, ed., *Engineering Electromagnetics*. Cham: Springer International Publishing, 2021.
[9] S. Loebel, T. Petzold, A. Martin, P. Steinert, A, Schubert, A. Thielecke, G. Meichsner, M. Hackert-Oschätzchen, R. Schulze, "Comparison of electrochemical removal characteristics between magnetized and demagnetized ndfeb," *The 18th International Symposium on Electrochemical Machining Technology (INSECT)*, vol. 2022, 2022.